Matter

Article

Establishing an elastic electron/lithium-ion transport network via *in situ* crosslinking for stabilizing interphases in SiO_x electrodes

Graphical abstract

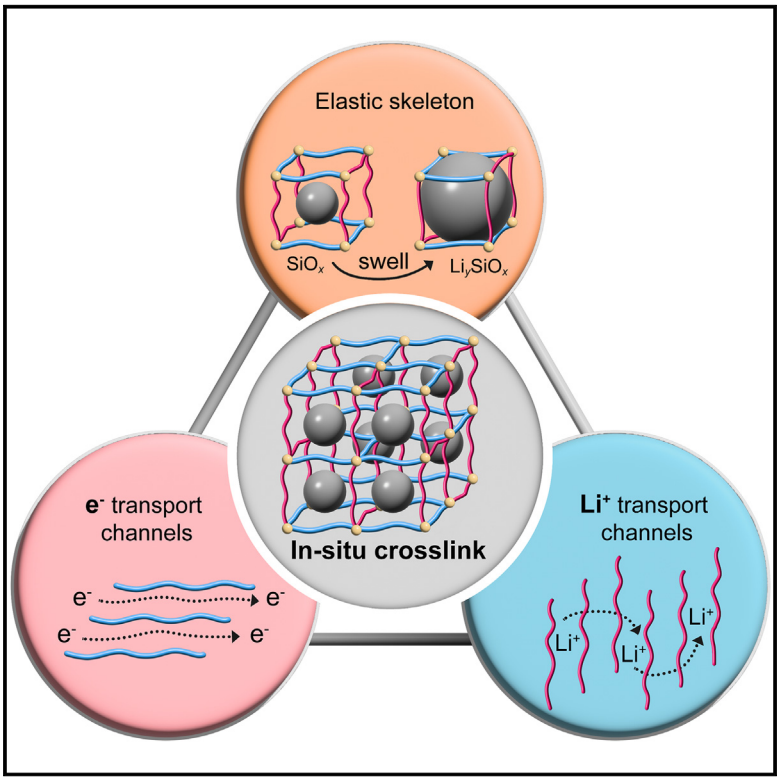

Highlights

- The *in-situ*-crosslinked conductive binder enables even dispersion of SiO_x particles
- The robust e^-/Li^+ transport network promotes the interfacial charge transfer
- The resilient network mitigates irreversible volume variation and SEI disintegration

Authors

Lu Wang, Zhibo Song, Yongsheng Li, ..., Tongchao Liu, Feng Pan, Luyi Yang

Correspondence

panfeng@pkusz.edu.cn (F.P.), yangly@pkusz.edu.cn (L.Y.)

In brief

By employing an *in situ* crosslinking strategy, a novel conductive binder is developed that serves as an elastic polymeric framework in SiO_x electrodes, providing a robust electron-permeation network and favorable interfacial lithium-ion transport pathways. As a result, the structural and interphasial stability of the anode is effectively maintained, leading to improved cycling stability and rate performance.

Wang et al., 2025, Matter *8*, 101952
May 7, 2025
https://doi.org/10.1016/j.matt.2024.101952

CellPress

Matter

CellPress

Article

Establishing an elastic electron/lithium-ion transport network via *in situ* crosslinking for stabilizing interphases in SiO_x electrodes

Lu Wang,[1] Zhibo Song,[1] Yongsheng Li,[1] Yuxiang Huang,[1] Hao Zhang,[1] Zuwei Yin,[2] Jinlin Xiao,[3] Chen Zhu,[1] Yiqian Zhao,[1] Meng Zhang,[3] Tongchao Liu,[4] Feng Pan,[1,*] and Luyi Yang[1,5,*]
[1]Shenzhen Graduate School, Peking University, Shenzhen 518055, China
[2]College of Energy, Xiamen University, Xiamen 361005, China
[3]BTR New Material Group Co., Ltd., Shenzhen 518107, China
[4]Argonne National Laboratory, Lemont, IL 60439, USA
[5]Lead contact
*Correspondence: panfeng@pkusz.edu.cn (F.P.), yangly@pkusz.edu.cn (L.Y.)
https://doi.org/10.1016/j.matt.2024.101952

PROGRESS AND POTENTIAL Silicon-based negative electrodes face limitations in fully utilizing their capacity due to the disruption of the conductive network and the degradation of the solid-electrolyte interphase (SEI) caused by significant volumetric effects. To date, achieving stable interfacial charge transfer while preserving the structural integrity of the electrode remains a significant challenge. Herein, based on a thiol-ene click reaction, a facile strategy is proposed to *in situ* construct a robust electron/Li^+ transport network for SiO_x electrodes. Exhibiting desirable mechanical strength and conductivity, this binding network not only achieves a stable SEI by mitigating the irreversible electrode volume variation but also provides uniformly distributed pathways for interfacial charge transport. This work proposes a modification strategy compatible with existing electrode fabrication processes, taking a step forward in the practical application of conductive binders in silicon-based anodes.

SUMMARY

The significant volumetric fluctuations experienced by high-capacity silicon-based electrodes during cycling lead to the disintegration of conductive frameworks and destabilization of the solid-electrolyte interphase (SEI). To overcome these challenges, an *in situ* thiol-ene click reaction is employed to fabricate an elastic electron/lithium-ion (e^-/Li^+)-conducting polymer network that uniformly binds SiO_x active materials. The proposed polymer incorporates rigid backbone segments that enhance electron conduction, along with flexible linkers that facilitate Li^+ transport and stress dissipation within the SiO_x electrode, thereby stabilizing the interfacial charge transfer on SiO_x. By reducing the initial expansion rate of the SiO_x electrode from 157% to 65%, the stable polymeric network effectively mitigates SEI degradation during cycling. As a result, the *in-situ*-crosslinked polymer framework enables improved capacity retention (82.7% after 250 cycles) and rate performance. By simultaneously strengthening the ion and electron transport pathways, this work offers new avenues for the future design of high-capacity negative electrodes.

INTRODUCTION

The pressing demand for high-energy-density and low-cost Li-ion batteries (LIBs) has been spurred by the fast development of electric vehicles and consumer electronic devices. One promising approach to meet such demand is to break through the capacity limit of intercalation-type graphite negative electrodes by using SiO_x ($0 < x < 2$), which exhibits high theoretical specific capacity, low redox potential, nontoxicity, and industrial scalability.[1–4] Despite these merits, SiO_x suffers from significant volume swings (~118%) during lithiation-delithiation processes, causing the unrestricted thickening of solid-electrolyte interphase (SEI) layers.[1,5] Such evolution eventually leads to the depletion of electrolytes and the breakdown of the electron percolating network, thus resulting in irreversible capacity loss.[2,3,6] Therefore, the key to preventing performance degradation is to suppress the free expansion/contraction of the electrode while maintaining the integrity of the interphasial carrier conduction network on SiO_x.

To stabilize the particle interphase, the development of high-performance polymer binders has become a key research focus

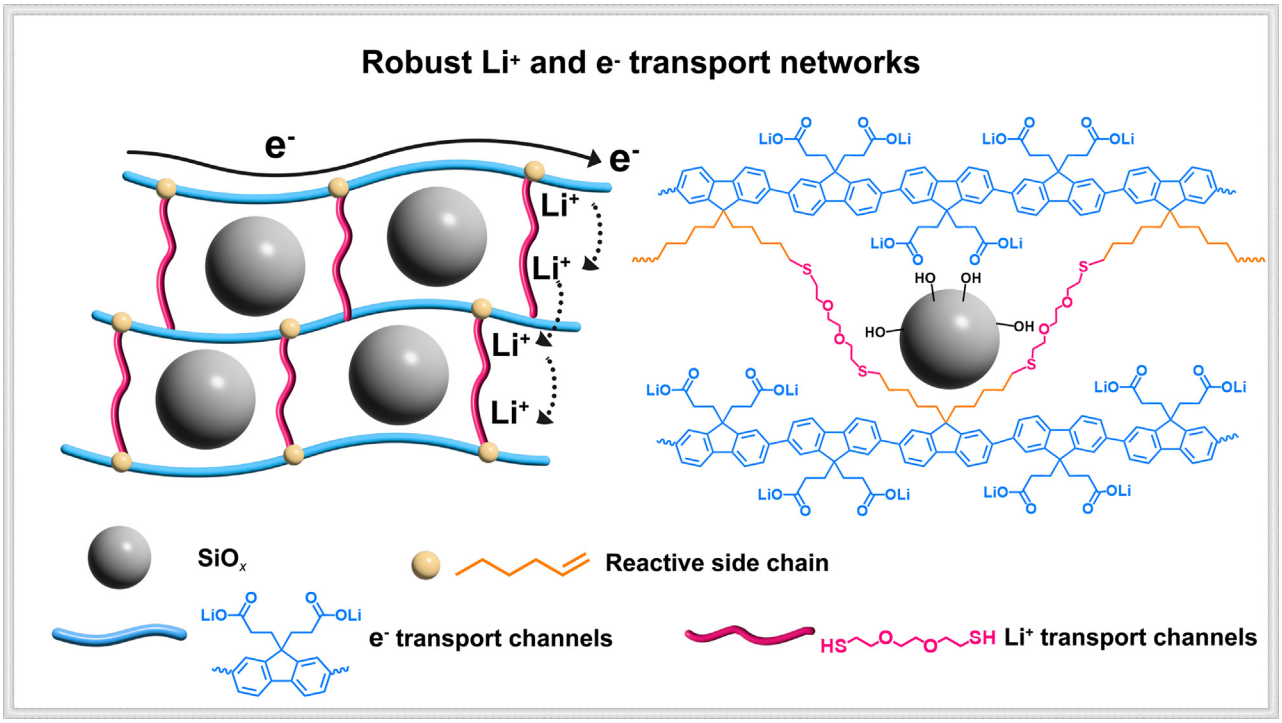

Figure 1. Architecting an elastic binding network to promote e^-/Li^+ transport via the proposed *in situ* photo-crosslinking strategy

for maintaining the high capacity of Si-based negative electrodes.[7–10] We have previously concluded that integrating high mechanical strength with high conductivity to binders is essential for Si-based negative electrodes[7,9]: on the one hand, the desirable mechanical strength could restrain the free expansion and contraction of the electrode (not particles) and enhance the structural adaptability of the anode particle interphase[11,12]; on the other hand, the conductive binder could provide an extra percolation network for electrons at the interphase of SiO_x.[13] However, it is difficult to significantly increase the molecular weight of conductive binders due to their rigid conjugated structures. Instead, it is much more feasible to increase the interaction between polymer chains, whose strength greatly affects the mechanical properties of the binder. One common strategy is to construct crosslinked networks through hydrogen bond, ionic bond, or covalent bond crosslinked polymers.[11,12,14,15] Nevertheless, crosslinked polymers are theoretically insoluble in commercially used solvents, resulting in poor dispersion of the slurry. Consequently, the contact between binders and active materials will be compromised, which not only prevents the polymeric conductive network from uniformly coating the active materials but also leads to uneven stress distribution during volume changes. Several prior reports have endeavored to facilitate crosslinking reactions during the mixing of slurries.[16,17] Nan et al. used polysaccharide polymers to construct a flexible polymer network for silicon-based electrodes under water bath heating conditions, resulting in improved performance.[18,19] Compared to the aforementioned methods, *in situ* crosslinking balances the advantages of active material dispersibility and reaction controllability, making it a more promising crosslinking approach.

To address above-mentioned issues, herein, a crosslinked electron/lithium-ion (e^-/Li^+) transport network is *in situ* constructed in an SiO_x anode electrode with the aid of a thiol-ene click reaction, which offers greater controllability compared with the thermo-crosslinking approach. The uncrosslinked conductive polymer facilitates good dispersion of active materials in the slurry, ensuring good homogeneity in the electrode. Upon crosslinking, the resultant polymer combines the flexibility of polyether segments and the rigidity of polyfluorene segments, creating a resilient binding network. Meanwhile, the electron percolation network constructed by the conjugated framework, along with the lithium-ion transport channels provided by the linker segments, ensure stable charge transfer in the anode (Figure 1). Owing to the improved elastic modulus (from 1.7 to 2.7 GPa), the first cycle expansion rate of the SiO_x electrode is significantly reduced from 157% to 65%. By integrating a series of morphological and componential characterizations,[20] the structural evolution SiO_x was also investigated. It is revealed that the *in-situ*-formed elastic polymeric network not only retains the structural integrity of the SiO_x electrodes but also contributes to maintain the stability of components and structures within the SEI. Taking advantage of this binder system, the SiO_x electrode exhibits superior electrochemical performance over electrodes using uncrosslinked and *ex-situ*-crosslinked binders.

RESULTS AND DISCUSSION

Architecting of elastic e^-/Li^+ transport network

Different from earlier studies where crosslinking processes take place during or before slurry mixing, the proposed *in situ*

crosslinking strategy is carried out after casting the slurry on the current collector. In this study, the ultraviolet (UV) light-initiated thiol-ene click reaction is chosen to drive the crosslinking reaction of the polymer chain due to its simplicity and speed, which are key factors for constructing a resilient confined network *in situ*. During the electrode drying process, the thiol crosslinkers in the slurry react with polyfluorene containing pentenyl and lithium propionate (PFDP-Li) under UV exposure to construct a three-dimensional (3D) network for e^-/Li^+ transport on the SiO_x particles (Figure 1). More specifically, the free radicals produced by the photoinitiator under UV light irradiation induce the production of sulfhydryl radicals, which undergo the addition reaction with the olefin group, thus crosslinking the linear conductive binder into a polymer network (see details in Figure S1).[21,22]

The (2,7-dibromo-9,9-di(pent-4-enyl)-9H-fluorene) monomer (M_{DP}) obtained by introducing the pentenyl group into 2,7-dibromofluorene (Figure S2) is characterized by the ^{1}H-nuclear magnetic resonance (^{1}H-NMR) spectrum (Figure S3). Exhibiting characteristic peaks of M_{DP}, the PFDP-Li segment synthesized by the Suzuki coupling reaction (Figure S4) can be distinguished from pristine polyfluorene containing lithium propionate (PF-Li) in Fourier transform infrared spectra (FTIR spectra) (Figure S5), where the appearance of the wagging vibration of $CH_2 = CH_2$ (914 cm^{-1}) confirms the introduction of monomer M_{DP}.[23,24] To determine the ideal UV radiation time for the thiol-ene click reaction, the FTIR spectra of PFDP-Li under different treatment durations are compared (Figure S6). The peak intensity of the ethylene-derived group at 912 cm^{-1} gradually decreases with UV irradiation time, indicating the continuous reaction between the thiol group of the crosslinking agent and the ethylenic bond.[23] After 20 min, the peak stops decreasing, suggesting the end of crosslinking reactions. Therefore, 20 min is chosen as the optimum UV treating time for this study. In addition, the degree of crosslinking is tested by X-ray photoelectron spectroscopy (XPS) measurements (Figure S7). With the addition of excessive thiol, except for the $2p_{1/2}$ and $2p_{3/2}$ peaks of the C–S bond, the S2p peaks of the unreacted thiol (–SH) appear at 160.50 and 161.68 eV, respectively, manifesting highly efficient *in situ* crosslinking of conductive polymers through the thiol-ene click reaction. The elemental distribution of the as-prepared electrode is analyzed by energy-dispersive spectroscopy (EDS). The uniform distribution of the S element on the electrode surface also suggests that crosslinking reactions occur homogeneously within the electrode (Figure S8). Time-of-flight secondary-ion mass spectroscopy (TOF-SIMS) measurements (Figure S9) were used to investigate the distribution of crosslinkers within the crosslinked binder. As expected, the fragments of the crosslinker chain are evenly distributed along with the conjugated backbone fragments, indicating the successful crosslinking process.

As shown with a nanoindentation test, the crosslinked PFDP-Li film exhibits a higher elastic modulus and hardness (Figure S10), demonstrating its potential capability to resist the free expansion of SiO_x electrodes. Similarly, through tensile performance testing (Figure S11), it was found that the crosslinking strategy increased the tensile modulus of the PFDP-Li film from 1.70 to 2.76 GPa, the yield strength from 17.42 to 87.85 MPa, and the tensile fracture strain by two times, suggesting that the crosslinked polymer membrane can store more elastic potential energy during the elastic deformation stage. Exhibiting superior mechanical properties, the constructed elastic crosslinked conductive network is more adaptable to the huge volume changes of anode materials during cycling, preventing the accumulation of internal stress and thereby reducing the risk of electrode cracking. Moreover, despite the introduction of unconjugated crosslinking agents, the two-probe tests show that the electronic conductivity of the polyfluorene film remains as high as 1.98×10^{-2} S cm^{-1} after crosslinking (Figure S12), which is sufficient for the purpose of interfacial electron conduction. The *in situ* photo-crosslinking approach facilitates the formation of a resilient percolating network for e^-/Li^+ transport.

Creating homogeneous e^-/Li^+ transport network for SiO_x electrodes

The uniform architecture of a polymer-confined network within the electrode is pivotal in realizing the full potential of high-capacity anodes. To evaluate the impact of *in situ* crosslinking on the electrode structure, we first compare the dispersing properties of uncrosslinked and *ex-situ*-crosslinked PFDP-Li binders. As shown in Figure S13, under UV light, the aqueous solution of the uncrosslinked PFDP-Li is uniformly dispersed and bright blue, while the aqueous solution of the *ex-situ*-crosslinked PFDP-Li is less transparent, with insoluble substances at the bottom, indicating that the crosslinked PFDP-Li cannot be uniformly dispersed in the slurry. The zeta potentials of SiO_x slurries prepared with the above two binders were measured to evaluate their dispersing properties. Figures 2A and S14 show that the absolute values of the zeta potentials in SiO_x slurries with *in-situ*-crosslinked PFDP-Li are much higher than those with *ex-situ*-crosslinked PFDP-Li, hence the better stability of the dispersion system. From the zeta potential distribution data (Figure S15), it can be further observed that the distribution peak of the *in-situ*-crosslinked slurry is narrower, indicating better uniformity of the particle surface potential and suppressed agglomeration.

As a damage-free characterization technique, nanocomputed tomography (nano-CT) was further employed to directly visualize the dispersion of SiO_x particles in different slurries. As shown in Figures 2B and S16, SiO_x particles in the slurries with uncrosslinked PFDP-Li exhibit an average equivalent diameter (eqdiameter) value of 3.16 μm and a median of 3.17 μm, with a narrow eqdiameter distribution around 2–4 μm. In comparison, the *ex-situ*-crosslinked group shows much larger particle sizes (average value = 4.64 μm and median value = 4.49 μm) as well as much wider size distribution, indicating a stronger tendency for particle agglomeration and poorer dispersion in the slurry. Similarly, the volume distribution histogram (Figure S17) also clearly shows that *ex situ* crosslinking leads to larger clusters of agglomerated SiO_x particles due to the poorly dissolved binder. The clustering of active materials not only impedes e^-/Li^+ conduction in the electrode but also causes larger local stress during the cycle, especially for materials with significant volume swings, eventually resulting in the collapse of the conductive network and thus seriously affecting the long cycle performance. Therefore, the *in situ* crosslinking strategy avoids such an issue by facilitating better SiO_x dispersion in the slurry.

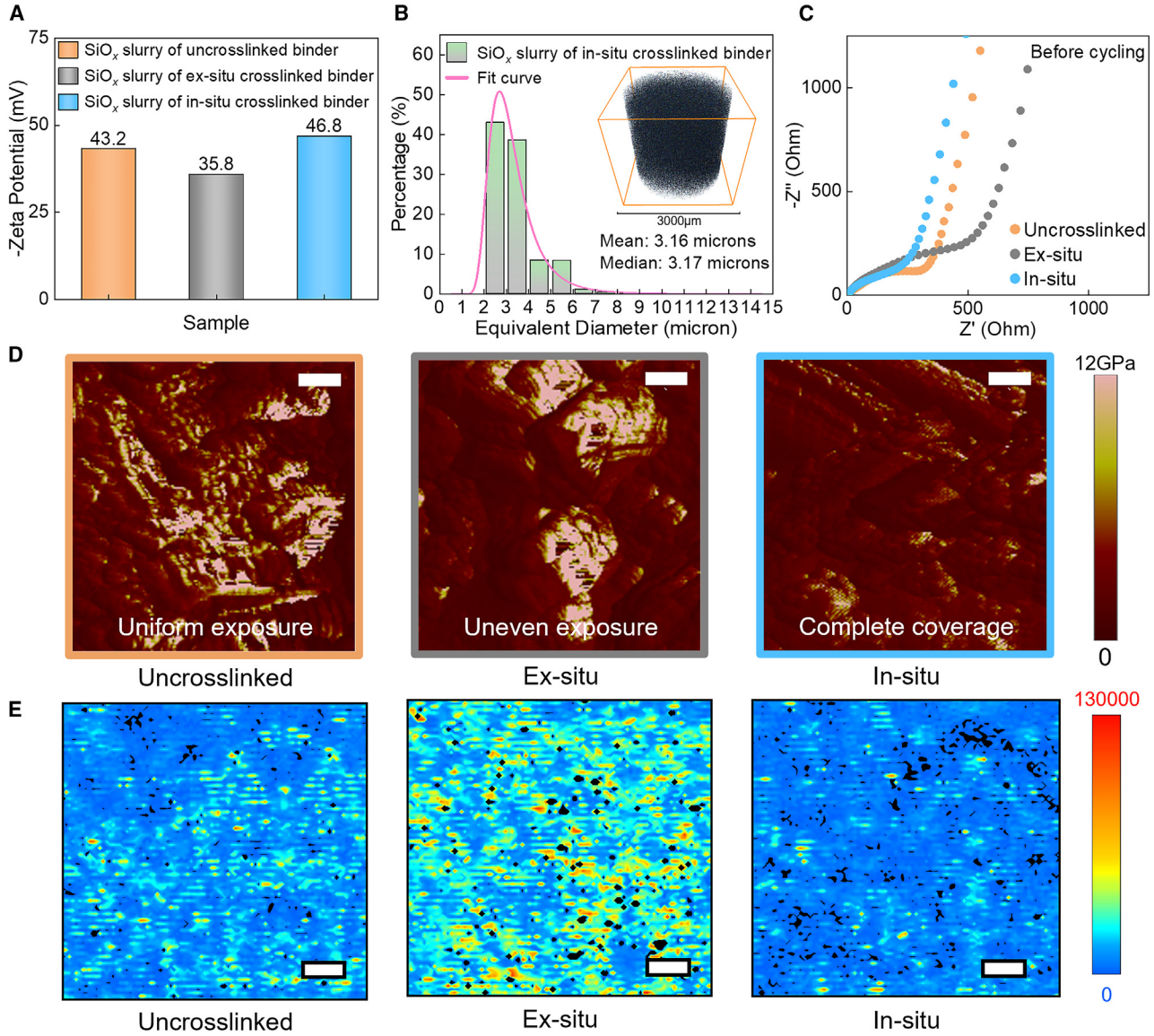

Figure 2. Creating homogeneous e^-/Li^+ transport network for SiO_x electrodes

(A) The zeta potential of SiO_x and different binders in water.

(B) The eqdiameter distribution histogram of SiO_x particle cluster in the slurry and nano-CT image (*in-situ*-crosslinked binder).

(C) Nyquist plots of the uncycled SiO_x electrodes with three different binders.

(D) DMT modulus mappings of the above three binder electrodes. The scale bars represent 300 nm.

(E) Raman mappings of pure SiO_x particle and the above three binder electrodes created by plotting the sum of the area of the Si Raman band as a function of position range from 430 to 530 cm^{-1}. The scale bars represent 20 μm.

Next, the electrochemical impedance spectra (Figure 2C) of the uncycled half-cells reveal that the *in-situ*-crosslinked electrode exhibits the lowest charge transfer resistance (R_{ct}). This improvement can be attributed to the promoted interfacial Li^+ transport facilitated by Li^+-solvating ether-oxygen segments.[25–29] In contrast, the *ex-situ*-crosslinked electrode, despite containing ether-oxygen segments, displays even higher R_{ct}. This is likely due to the uneven binder dispersion, which hinders the formation of a fully wetted electrolyte-anode interface. Moreover, FTIR spectroscopy results (Figure S18) show that the –COOLi groups in the conductive binder will form ester bonds with the hydroxyl (–OH) groups on the surface of SiO_x particles in the process of heating and drying electrodes so that the conductive binder can firmly anchor to the SiO_x particles to maintain a connected e^-/Li^+ transport network.

The stripping test (Figure S19) first proves that the uneven distribution of the binder caused by the *ex situ* crosslinking directly affects adhesion to the SiO_x particles and copper foil. Besides, the *in-situ*-crosslinked SiO_x electrode exhibits the highest shear force, which is attributed to the firm binding between the

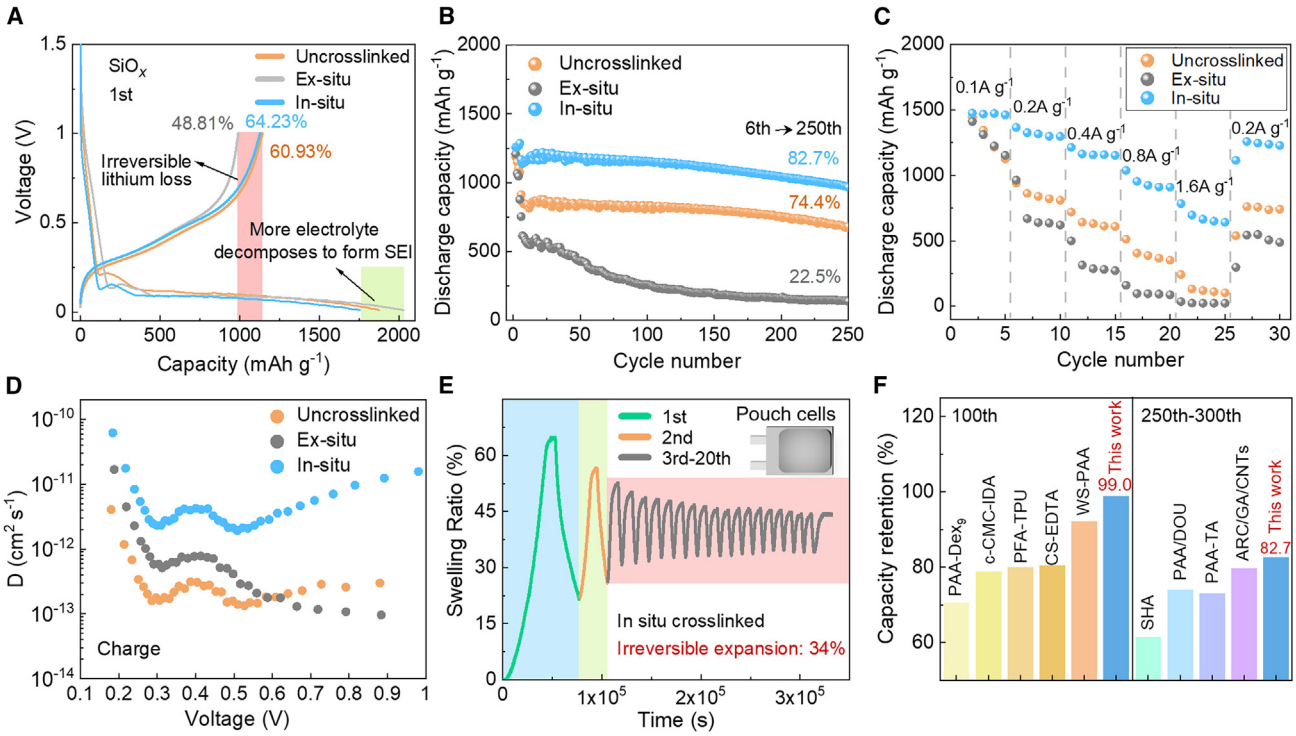

Figure 3. Improving the electrochemical performance of SiO_x electrodes

(A) Initial galvanostatic discharge/charge profiles (0.2 A g^{-1}) of SiO_x electrodes using different binders.

(B) Cycling performance of SiO_x electrodes using different binders at a current density of 0.4 A g^{-1}.

(C) Rate performance of SiO_x electrodes using different binders.

(D) The calculated Li^+ diffusion coefficients of the SiO_x electrodes during charge processes from the GITT curves.

(E) Expansion rate curves of *in-situ*-crosslinked electrodes.

(F) Comparison of capacity retention of the *in-situ*-crosslinked electrode with recently reported advanced SiO_x electrodes.

mercaptan short chain and the conjugated long chain. Further, atomic force microscopy (AFM) is used to study the homogeneity of binder coatings on the surface of SiO_x electrodes. Derjaguin-Muller-Toporov (DMT) modulus mappings (Figures 2D and S20) show that there are obvious areas with high moduli on the surface of both uncrosslinked PFDP-Li and *ex-situ*-crosslinked PFDP-Li electrodes, indicating that SiO_x particles are not fully embedded in the polymer network, which might trigger uneven internal stress caused by the volume change inside the electrode. In contrast, the surface of the *in-situ*-crosslinked electrode exhibits the DMT modulus value of the binder, indicating that under UV light irradiation, the thiol crosslinker weaves the conductive polymer onto the surface of SiO_x particles to form a uniform and complete 3D elastic network, ensuring the structural stability of the electrode while providing internal electron and Li^+ transport channels. This result is verified by Raman spectroscopy mapping of electrodes using different binders (Figure 2E), where the signals corresponding to Si (Figure S21) are prominent for both uncrosslinked and *ex-situ*-crosslinked binders, whereas Si signals can barely be detected on the *in-situ*-crosslinked electrode. Besides, the bending experiment (Figure S22) of the electrodes shows that the *in situ* crosslinking strategy constructs a uniform elastic binder network, which avoids electrode cracking and maintains the integrity of the electrode. Therefore, it can be concluded that with the help of the thiol-ene click reaction, a homogeneous conductive crosslinked network with great mechanical properties can be constructed *in situ* in the manufacturing process of commercial electrodes.

Improving the electrochemical performance of SiO_x electrodes

The advantage of the uniformly confined e^-/Li^+ transport network is directly manifested in the enhanced electrochemical performance of the SiO_x anode. Galvanostatic charge-discharge tests of SiO_x electrodes using uncrosslinked, *in-situ*-crosslinked, and *ex-situ*-crosslinked PFDP-Li binders were carried out in half-cells to assess the electrochemical performance. The amount of crosslinker directly affects the degree of crosslinking of the binder network, which determines the electrochemical performance of the SiO_x electrode. Based on the cycling stability, the optimal amass ratio of uncrosslinked binder to crosslinker is determined to be 20:1 (Figure S23). The first cycle voltage profile (Figure 3A) shows that the *in-situ*-crosslinked SiO_x electrode exhibits the highest initial coulombic efficiency (ICE), which could be due to the least exposed SiO_x surface. Long-term cycling performance (Figure 3B) shows that the *in-situ*-crosslinked electrode exhibits a specific capacity of 967 mAh g^{-1} after 250 cycles, corresponding to a higher capacity retention rate of

82.7%, which outperforms both the uncrosslinked (680 mAh g^{-1}, 74.4%) and *ex-situ*-crosslinked (138 mAh g^{-1}, 22.5%) SiO_x electrodes. Similarly, the *in situ* crosslinking strategy is also effective for promoting the performance of Si electrodes (Figure S24). Additionally, it can be observed that the *in-situ*-crosslinked electrode has the lowest overpotential after 100 cycles (Figure S25), indicating that the construction of a robust yet homogeneous conductive network to ensure electron conduction is essential for lowering the voltage polarization. The coulombic efficiency variation curves (Figure S26) also show that the coulombic efficiency of the *in-situ*-crosslinked electrode gradually increased to 98% over 7 cycles and stabilized over 99% in sequential cycles, suggesting the formation of a stable SEI. In contrast, the coulombic efficiency curve of the *ex-situ*-crosslinked electrode fluctuated during cycling, which might be due to the uneven SEI growth on aggregated SiO_x particles. As a result, the repeated formation-destruction of the SEI causes a thicker interfacial layer. This speculation is confirmed by the electrochemical impedance spectra, where the SEI layer resistance (R_{SEI}) and the R_{ct} of the *ex-situ*-crosslinked electrode are much higher than those of the other two electrodes, whereas the *in-situ*-crosslinked electrode exhibits the lowest R_{SEI} and R_{ct} (Figure S27; Table S1). The elastic conductive polymer network suppresses interphasial aging of SiO_x particles, which allows a fast charge transfer process. Consequently, the *in-situ*-crosslinked binder also facilitates a superior rate performance of Si-based negative electrode materials (Figures 3C and S28). Galvanostatic intermittent titration (GITT) tests also show that the *in-situ*-crosslinked electrode has a higher Li^+ diffusion coefficient (Figures 3D and S29), which can only be contributed by the interphasial area of SiO_x.

To unveil the role of *in situ* crosslinking in reinforcing the electrode structures, *in situ* expansion tests were conducted in full cells (Tables S2 and S3). The results (Figures 3E and S30) show that the highest expansion rate of SiO_x electrodes during the first lithium insertion process are 65% (*in situ*) and 58% (*ex situ*), respectively. By sharp contrast, the highest expansion rate of the uncrosslinked electrode is 157%, which is due to the weak polymer interactions being unable to withstand the volume change, causing the collapse of the binding network. In the subsequent cycles (3rd–20th), the *in-situ*-crosslinked electrode exhibits lower irreversible expansion compared with the *ex-situ*-crosslinked one. It is speculated that the aggregation of the *ex-situ*-crosslinked polymer is unable to evenly dissipate internal stress around the particles, resulting in destructive cracking inside the electrode. The *in situ* photo-crosslinking strategy constructs a uniform confined polymer framework at the particle interface, which avoids stress concentration and exhibits excellent stress dissipation ability. Owing to the complete e^-/Li^+ permeation network, the *in-situ*-crosslinked electrode exhibits improved capacity retention (≈99% after 100 cycles) compared to recently reported advanced SiO_x electrodes (Figure 3F; Table S4).[30–38]

Enhancing the bulk structural stability of electrodes during cycling

The superior performance of the SiO_x anode is fundamentally attributed to the elastic framework formed by the rigid main chains and flexible linker chains intertwining, which plays a crucial role in stabilizing the bulk structure of the electrode. A scanning electron microscope (SEM) was used to examine the surface morphology of SiO_x electrodes after cycling (Figure S31). After a long period of cycling, a smooth surface without any apparent cracks can be observed on the *in-situ*-crosslinked electrode. By sharp contrast, there are many large cracks on the uncrosslinked electrode surface, which is caused by the low modulus of the uncrosslinked binder that cannot withstand large volume changes. As for the *ex-situ*-crosslinked electrode, due to the ineffective binding, although there is no obvious cracking on the surface of the electrode, a large amount of internal SiO_x particles are separated from the conductive network, resulting in the capacity fading. Similar phenomena can also be observed on Si electrodes (Figure S32), where fractured surfaces can be observed on both uncrosslinked and *ex-situ*-crosslinked electrodes. The DMT mappings (Figure S33) of the cycled electrode also indicate that the *in situ* crosslinking method can firmly bond the particles in the electrode. There are obvious exposed SiO_x particles on the surface of the uncrosslinked and *ex-situ*-crosslinked electrode sheets due to detachment from the bonding. Moreover, according to the 3D surface morphology of the electrodes (Figure S34), the *in situ* crosslinking strategy results in the smallest surface roughness of the electrode, further confirming that the homogeneity of *in-situ*-crosslinked electrodes can be well retained after long-term cycling.

The distribution of organic components, inorganic particles, and voids in the SiO_x electrodes under different stages (0th, 50th, 150th), as well as the structural evolution of the electrodes from macroscopic to mesoscopic, were characterized by focused ion beam and SEM (FIB-SEM) technology.[5,39] Firstly, the evolution of component proportions in three types of electrodes with different numbers of cycles was analyzed (Figure 4A). For the electrodes before cycling, the component proportions in the *in-situ*-crosslinked and uncrosslinked electrodes are similar, suggesting that the *in situ* crosslinking process has not affected the dispersibility of active materials within the electrode, whereas the proportion of the active materials in the *ex-situ*-crosslinked electrodes is higher due to the poor dispersion of particles. After 150 cycles, the proportion of voids in the uncrosslinked electrode becomes higher, which corresponds to its high irreversible expansion. As for the electrode with the *ex-situ*-crosslinked binder, although its structure has not become as porous as the uncrosslinked group, a distinctive increase of organic species can be clearly observed, which is predominantly contributed by SEI thickening. Both cases above will inevitably result in the breakdown of electron percolation networks. Due to the formation of a robust binding network, issues of SEI aging and electrode breakdown have been effectively alleviated in the *in-situ*-crosslinked electrode, where the percentage of active material remain constant. Furthermore, the 3D-reconstructed images of the electrodes (Figures S35–S37) agree with the above quantitative results: porosity generation and SEI growth can be clearly observed in uncrosslinked and *ex-situ*-crosslinked electrodes, respectively, while the electrodes prepared by *in situ* crosslinking technology have more uniform particle dispersion throughout the cycling. Next, the eqdiameter distribution in the 3D-reconstructed image model is used to analyze the evolution

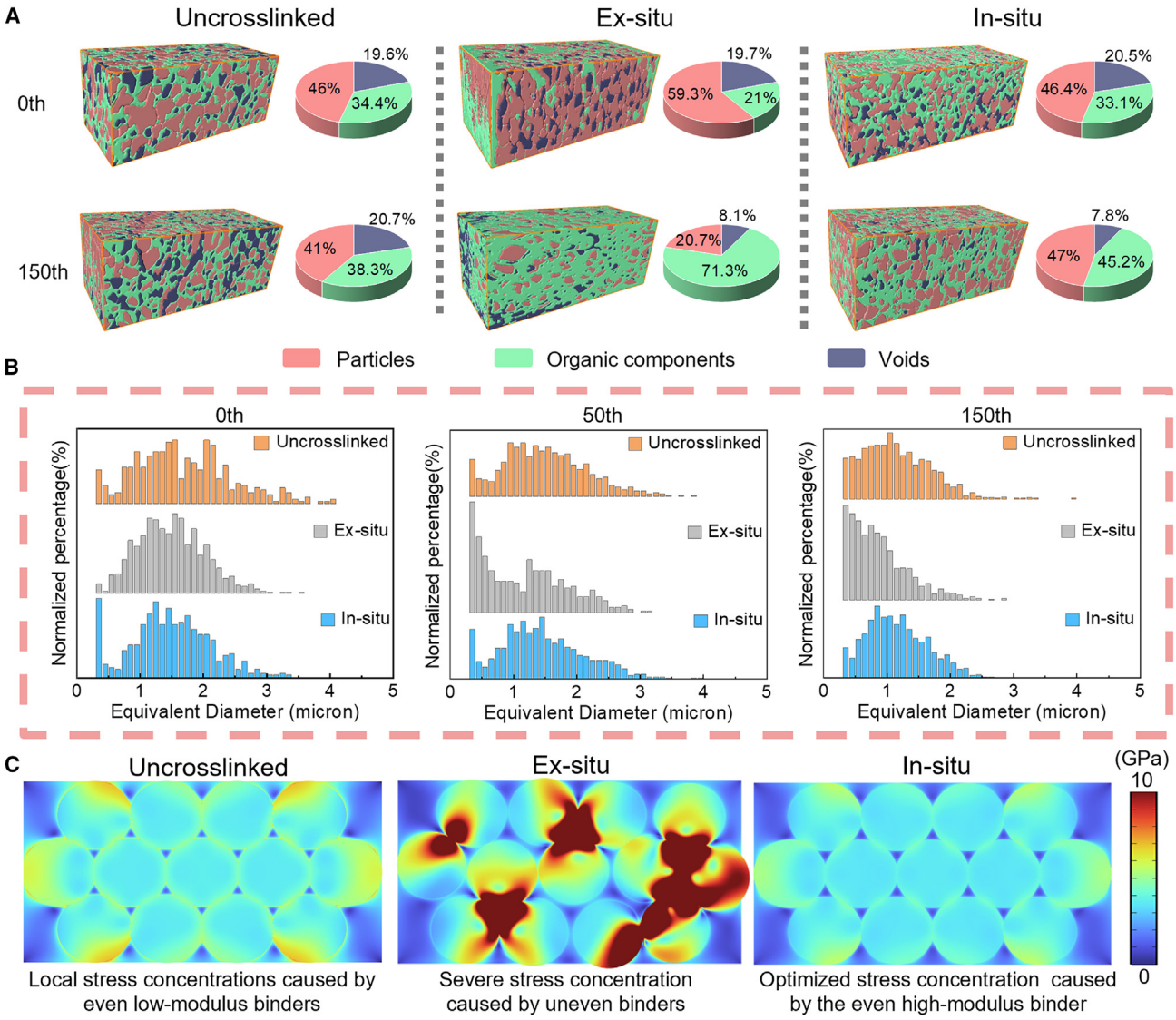

Figure 4. Enhancing the bulk structural stability of electrodes during cycling

(A and B) The evolution of the components in the electrode with cycling is explored, especially the pulverization of SiO_x particles in different electrodes. The FIB-SEM test and 3D reconstruction are used to obtain (A) the volume proportion of particles, organic components, and voids in the electrodes before and after cycling and (B) the internal particle size distribution curves for the electrodes at different cycles.

(C) Stress distribution pattern inside the electrodes at the initial lithiation state, simulated by the finite element method.

of particles (Figure 4B). It can be clearly seen that during cycling, the particle sizes in the *in-situ*-crosslinked electrode remained constant, while smaller particles emerged in the other two electrodes, especially for the *ex-situ*-crosslinked group. This phenomenon is generally related to the pulverization of SiO_x particles.

To further understand the role of binders in SiO_x electrodes, finite element simulation was used to demonstrate the stress distribution inside the electrode after lithiation. Based on previous reports and relevant experimental results,[40,41] the simulation parameters are displayed in Table S5. Subsequently, geometric models (Figure S38) of uncrosslinking, *in situ* crosslinking, and *ex situ* crosslinking systems were established. As shown in Figure 4C, firstly, the ability of linear polymers to resist deformation and their own toughness increase after crosslinking, resulting in lower internal stress in the *in-situ*-crosslinked electrodes. Owing to the lower elastic modulus of the linear PFDA-Li, a marginally high stress concentration is present around the SiO_x particles of the uncrosslinked electrodes. However, for *ex-situ*-crosslinked electrodes, although the mechanical properties of the binder have been improved, the poor dispersion of SiO_x particles results in uneven stress distribution and high stress concentration within the electrode. Especially in areas lacking binder protection, the high stress concentration of particles induces particle crushing. Therefore, simply improving the mechanical properties of the binder alone is not enough, and it is equally

important to improve the dispersion of each component in the electrode. The elastic framework constructed by the *in situ* crosslinking strategy uniformly encapsulates the SiO_x particles in the electrode, avoiding the rapid degradation of performance caused by severe pulverization.

Reinforcing the interphasial stability of the SiO_x electrodes

As two dominating components covering the surface of negative electrode materials, the correlation and interplay between the binder and SEI have barely been investigated. Herein, an in-depth investigation of the SEI on different electrodes after cycling was conducted using XPS (Figures 5A and S39). The uncrosslinked electrode surface SEI has more Li_2CO_3/$ROCO_2Li$ and LiF derived from the decomposition of fluoroethylene carbonate (FEC) and ethylene carbonate (EC) in the electrolyte[42,43] and also contains some $Li_xPO_yF_z$ derived from the incomplete decomposition of $LiPF_6$, indicating that the uncrosslinked PFDP-Li fails to effectively protect the surface of the SiO_x particles from persistent side reactions. For the *ex-situ*-crosslinked group, the higher C–O peak and $Li_xPO_yF_z$ peak reflect a significant amount of undesirable components with poor mechanical properties, making the SEI unable to adapt to repeated particle expansion. Furthermore, in the Si2p spectrum, a clear Si–O peak can be observed (Figure S40), corresponding to the exposed SiO_x particle surface due to the fragile SEI.[43,44] By sharp contrast, the SEI of the *in-situ*-crosslinked electrode contains more inorganic components (e.g., LiF) and less carbonate-derived species. Such chemical constitutes bear more resemblance to the components of the SEI formed at the early stages, indicating a well-maintained SEI throughout prolonged cycling. Similarly, the O K-edge soft X-ray absorption spectroscopy (sXAS) data were collected in both total electron yield (TEY) mode and partial fluorescence yield (PFY) mode to explore the surface and bulk information of the electrode, respectively (Figures 5B and S41). Both TEY and PFY spectra show that the surface oxygen compounds of the *ex-situ*-crosslinked electrode contain a large amount of organic components (lithium carboxylate: LEMC, LEDC),[45,46] while the surfaces of the other two consist of a large number of inorganic components (Li_2CO_3) and a small amount of lithium carboxylate. Compared with the *in-situ*-crosslinked electrode, the SEI of the uncrosslinked electrode has more Li_2CO_3 on the outer layer and relatively more organic lithium carboxylate components on the inner layer. The test results are consistent with the SEI information provided by XPS. Besides, molecular dynamics (MD) simulations were conducted to further investigate the effect of binders on the solvation structures of nearby lithium ions, thereby interfering with the formation of the SEI (Figure S42). In the presence of the binder, FEC is more likely to enter the first solvation shell of Li^+, excluding EC molecules from the sheath. Therefore, ensuring the widespread and uniform presence of the binder on the SiO_x surface can facilitate the formation of homogeneous LiF-rich SEI components through the decomposition of FEC.

Based on results above, the impact of the binder on SEI formation for SiO_x is schematically illustrated in Figure 5C. During the initial cycle, FEC reacts near the conductive binder to produce LiF and Li_2CO_3, which, together with the binder, consititute the inner layer of the SEI (Figure S43). As the reaction progresses, the electrolyte derivatives persist in growing upon the inner layer to construct the initial SEI layer. To better illustrate the evolution of the SEI, we performed compositional characterization of the SEI at different cycle numbers (Figure S44). During long-term cycling, although the uncrosslinked polymer is well coated on the surface of the particles, as the SiO_x particles expand, the surface polymer molecules are detached from each other due to the weak binding, resulting in irreversible volume variations of SiO_x electrodes (as depicted in Figure S30), as well as SEI thickening. Consequently, LiF content that mainly originated from the decomposition of the FEC additive will eventually be diluted by Li_2CO_3 as the depletion of FEC owing to the persistent side reactions. On the other hand, although the mechanical properties of the binder can be improved by *ex situ* crosslinking, the poor dispersion of crosslinked polymers causes the inhomogeneous lithiation/delithiation of SiO_x particles, as well as severe non-uniform stress within the electrode. Additionally, as mentioned above, although FEC tends to form LiF on the surface of the binder, the uneven distribution of the binder prevents LiF from uniformly coating the active material, resulting in an SEI with non-uniform mechanical properties and lithium-ion conductivity. In this case, the uneven binder-inorganic inner layer fails to maintain a homogeneous interphase for SiO_x, leading to continuous side reactions for EC and $LiPF_6$. In contrast, the *in situ* photo-crosslinking technique constructs a 3D skeleton and a uniform e^-/Li^+ transport network inside. The former stabilizes the SEI inner layer and thus avoids the thickening of SEI, whereas the latter allows the SiO_x particles to undergo uniform volume changes, preventing stress concentration on the surface. As a consequence, a LiF-rich interphase could be preserved, which not only promotes interphasial Li^+ transport but also passivates the particle surface to minimize parasitic reactions.[42] Moreover, a homogeneous LiF-rich SEI could better tolerate the drastic deformation of Si-based electrodes due to the high Young's modulus and low adhesion to the SiO_x surface,[43,47] which works synergistically with the binder to maintain the structural stability of SiO_x electrodes.

Based on the above results, the improved mechanism of the proposed polymer network on the SiO_x anode can be divided into the following aspects (Figure 6). Through *in situ* crosslinking, a polymer composed of a rigid electronic conductive framework and flexible Li^+-conducting crosslinking units forms a robust binding network on the surface of SiO_x via covalent bonding. With its intrinsic high mechanical strength and conductivity, the polymer we developed not only realizes better stress dissipation and constrains the irreversible volume changes of the electrode but also provides additional interfacial charge transfer pathways to enable uniform lithiation and delithiation. Moreover, the *in-situ*-crosslinked binder contributes to SEI stability in two ways: on one hand, the uniformly distributed binder can induce FEC to enter the solvation sheath of Li^+, forming a LiF-rich SEI; on the other hand, the limited space for growth restricts the repeated thickening of the SEI.

Conclusion

In summary, *in situ* photo-crosslinked binder technology suitable for large-scale preparation of electrodes was proposed,

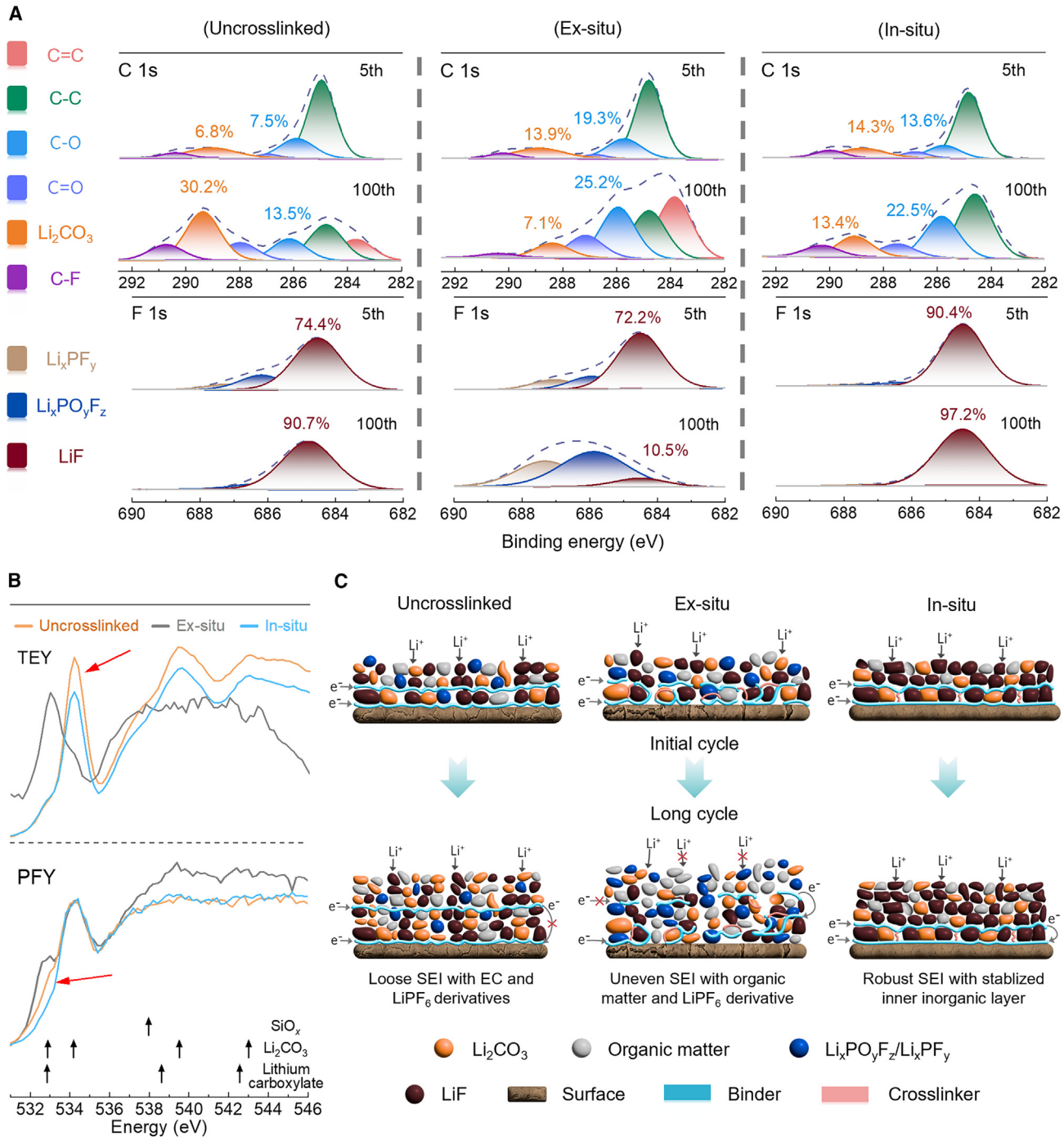

Figure 5. Reinforcing the interphasial stability of the SiO_x electrodes

(A) High-resolution XPS C 1s and F 1s spectra of different SiO_x electrodes after 5 and 100 cycles.

(B) O K-edge sXAS TEY/PFY spectra of three electrodes after 100 cycles.

(C) Schematic diagram depicts the effect of the different protective abilities of binders on the surface of SiO_x particles on the SEI composition.

improving the performance of SiO_x electrodes by stabilizing the bulk phase and interface. Firstly, an even 3D elastic conductive network with alternating rigid and flexible segments is constructed *in situ* in the SiO_x electrode, inhibiting the expansion rate of the electrode and alleviating the irreversible pulverization of SiO_x particles inside the electrode. With the help of nano-CT and FIB-SEM 3D reconstruction technology, it has been proven that the uniformity of the polymer layer on the particle surface

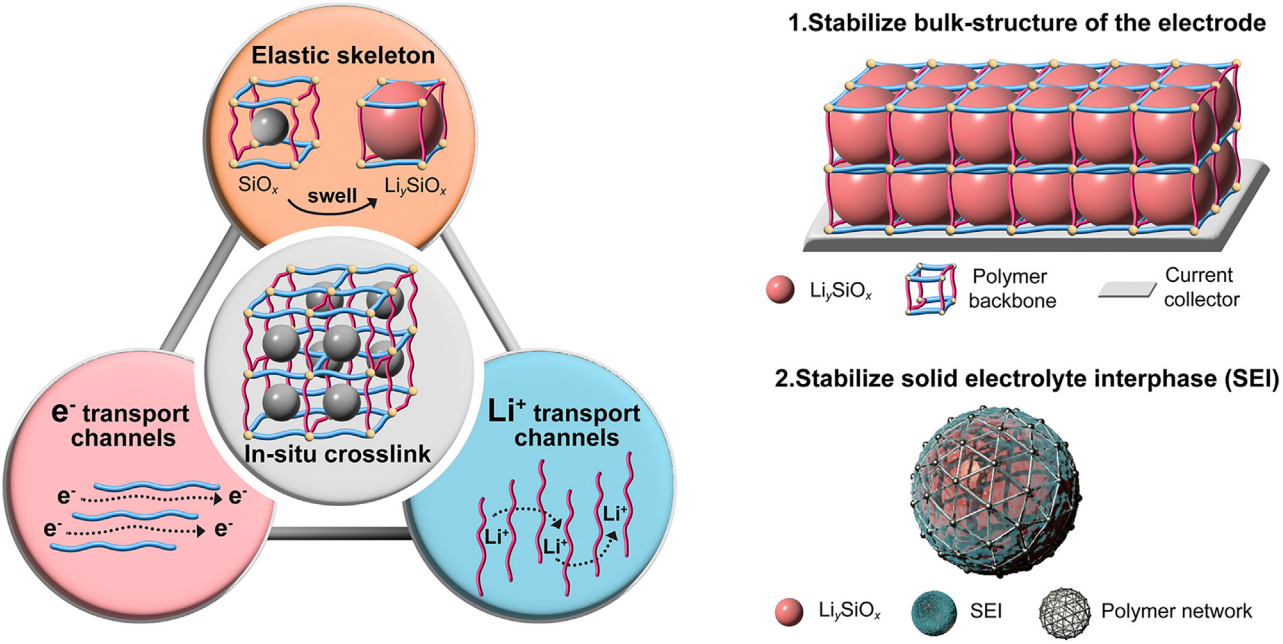

Figure 6. Schematic illustration for the mechanism of maximizing the high performance of the SiO_x electrodes through the constructed trifunctional binder network using the *in situ* crosslinking strategy

cannot be neglected when developing high-performance binders, as it directly affects the uniformity of the electrode and the integrity of SiO_x particles during repeated expansion. As demonstrated in the results of XPS and sXAS, by confining the free expansion-contraction process of SiO_x, the associated electrolyte decomposition is also minimized, effectively preserving the stability of components and structure within the SEI. By constructing an e^-/Li^+ transport network *in situ* on the particle surface through a readily scalable electrode preparation method, this study simultaneously modulated the charge conduction and mechanical stability of the SiO_x negative electrode, offering new insights for the design of high-capacity negative electrodes.

METHODS

Details regarding the experimental procedures can be found in the supplemental methods.

RESOURCE AVAILABILITY

Lead contact

Further information and requests for resources and reagents should be directed to and will be fulfilled by the lead contact, Luyi Yang (yangly@pkusz.edu.cn).

Materials availability

This study did not generate new unique reagents.

Data and code availability

This study did not generate any datasets.

ACKNOWLEDGMENTS

L.Y. acknowledges financial support from the National Natural Science Foundation of China (no. 52303263). F.P. acknowledges financial support from the Shenzhen Key Laboratory of New Energy Resources Genome Preparation and Testing (no. ZDSYS201707281026184), the International Joint Research Center for Electric Vehicle Power Battery and Materials (no. 2015B01015), and the Guangdong Key Laboratory of Design and Calculation of New Energy Materials (no. 2017B030301013). The authors thank the support from the Shanghai Synchrotron Radiation Facility (SSRF) (beamline 02B02).

AUTHOR CONTRIBUTIONS

L.W. and L.Y. conceived and designed the experiments. L.Y. and F.P. directed the project. L.W. and Z.S. prepared the materials and performed the electrochemical testing. Y.L. and C.Z. conducted the FIB-SEM characterization. H.Z. performed the Raman measurements. J.X. and M.Z. performed the electrode expansion measurements. Y.H. conducted the AFM measurements. Y.Z. tested the mechanical properties of the polymer. L.W., L.Y., and T.L. analyzed the data. L.W., T.L., and L.Y. wrote the paper. F.P., L.Y., and T.L. provided materials and characterization tools. F.P. and L.Y. polished the writing. All authors discussed the results and commented on the manuscript.

DECLARATION OF INTERESTS

The authors declare no competing interests.

SUPPLEMENTAL INFORMATION

Supplemental information can be found online at https://doi.org/10.1016/j.matt.2024.101952.

Received: September 27, 2024
Revised: November 27, 2024
Accepted: December 19, 2024
Published: January 21, 2025

REFERENCES

1. Liu, Z., Yu, Q., Zhao, Y., He, R., Xu, M., Feng, S., Li, S., Zhou, L., and Mai, L. (2019). Silicon oxides: a promising family of anode materials for lithium-ion batteries. Chem. Soc. Rev. *48*, 285–309. https://doi.org/10.1039/c8cs00441b.
2. Li, P., Zhao, G., Zheng, X., Xu, X., Yao, C., Sun, W., and Dou, S.X. (2018). Recent progress on silicon-based anode materials for practical lithium-ion battery applications. Energy Storage Mater. *15*, 422–446. https://doi.org/10.1016/j.ensm.2018.07.014.
3. Zhu, G., Chao, D., Xu, W., Wu, M., and Zhang, H. (2021). Microscale silicon-based anodes: Fundamental understanding and industrial prospects for practical high-energy lithium-ion batteries. ACS Nano *15*, 15567–15593. https://doi.org/10.1021/acsnano.1c05898.
4. Chen, Z., Soltani, A., Chen, Y., Zhang, Q., Davoodi, A., Hosseinpour, S., Peukert, W., and Liu, W. (2022). Emerging organic surface chemistry for Si anodes in lithium-ion batteries: Advances, prospects, and beyond. Adv. Energy Mater. *12*, 2200924. https://doi.org/10.1002/aenm.202200924.
5. Qian, G., Li, Y., Chen, H., Xie, L., Liu, T., Yang, N., Song, Y., Lin, C., Cheng, J., Nakashima, N., et al. (2023). Revealing the aging process of solid electrolyte interphase on SiOx anode. Nat. Commun. *14*, 6048. https://doi.org/10.1038/s41467-023-41867-6.
6. He, Y., Jiang, L., Chen, T., Xu, Y., Jia, H., Yi, R., Xue, D., Song, M., Genc, A., Bouchet-Marquis, C., et al. (2021). Progressive growth of the solid-electrolyte interphase towards the Si anode interior causes capacity fading. Nat. Nanotechnol. *16*, 1113–1120. https://doi.org/10.1038/s41565-021-00947-8.
7. Chen, S., Song, Z., Wang, L., Chen, H., Zhang, S., Pan, F., and Yang, L. (2022). Establishing a resilient conductive binding network for Si-based anodes via molecular engineering. Acc. Chem. Res. *55*, 2088–2102. https://doi.org/10.1021/acs.accounts.2c00259.
8. Liu, Y., Shao, R., Jiang, R., Song, X., Jin, Z., and Sun, L. (2023). A review of existing and emerging binders for silicon anodic Li-ion batteries. Nano Res. *16*, 6736–6752. https://doi.org/10.1007/s12274-022-5281-7.
9. Song, Z., Wang, L., Yang, K., Gong, Y., Yang, L., Liu, X., and Pan, F. (2022). Intermolecular chemistry for designing functional binders in silicon/carbon composite anodes. Mater. Today Energy *30*, 101153. https://doi.org/10.1016/j.mtener.2022.101153.
10. Li, Z., Du, M., Guo, X., Zhang, D., Wang, Q., Sun, H., Wang, B., and Wu, Y.A. (2023). Research progress of SiOx-based anode materials for lithium-ion batteries. Chem. Eng. J. *473*, 145294. https://doi.org/10.1016/j.cej.2023.145294.
11. Song, Z., Chen, S., Zhao, Y., Xue, S., Qian, G., Fang, J., Zhang, T., Long, C., Yang, L., and Pan, F. (2021). Constructing a resilient hierarchical conductive network to promote cycling stability of SiOx anode via binder design. Small *17*, 2102256. https://doi.org/10.1002/smll.202102256.
12. Song, Z., Zhang, T., Wang, L., Zhao, Y., Li, Z., Zhang, M., Wang, K., Xue, S., Fang, J., Ji, Y., et al. (2022). Bio-inspired binder design for a robust conductive network in silicon-based anodes. Small Methods *6*, 2101591. https://doi.org/10.1002/smtd.202101591.
13. Liu, D., Zhao, Y., Tan, R., Tian, L.L., Liu, Y.D., Chen, H.B., and Pan, F. (2017). Novel conductive binder for high-performance silicon anodes in lithium ion batteries. Nano Energy *36*, 206–212. https://doi.org/10.1016/j.nanoen.2017.04.043.
14. Liu, X., Iqbal, A., Ali, N., Qi, R., and Qian, X. (2020). Ion-cross-linking-promoted high-performance Si/PEDOT:PSS electrodes: The importance of cations' ionic potential and softness parameters. ACS Appl. Mater. Interfaces *12*, 19431–19438. https://doi.org/10.1021/acsami.0c00755.
15. Zhang, B., Dong, Y., Han, J., Zhen, Y., Hu, C., and Liu, D. (2023). Physicochemical dual cross-linking conductive polymeric networks combining high strength and high toughness enable stable operation of silicon microparticle anodes. Adv. Mater. *35*, e2301320. https://doi.org/10.1002/adma.202301320.
16. Zhu, X., Zhang, F., Zhang, L., Zhang, L., Song, Y., Jiang, T., Sayed, S., Lu, C., Wang, X., Sun, J., and Liu, Z. (2018). A highly stretchable cross-linked polyacrylamide hydrogel as an effective binder for silicon and sulfur electrodes toward durable lithium-ion storage. Adv. Funct. Mater. *28*, 1705015. https://doi.org/10.1002/adfm.201705015.
17. Kuo, T.-C., Chiou, C.-Y., Li, C.-C., and Lee, J.-T. (2019). In situ cross-linked poly(ether urethane) elastomer as a binder for high-performance Si anodes of lithium-ion batteries. Electrochim. Acta *327*, 135011. https://doi.org/10.1016/j.electacta.2019.135011.
18. Liu, H., Liao, J., Zhu, T., Ma, Z., Zhao, X., and Nan, J. (2023). In situ hydrogel polymerization to form a flexible polysaccharide synergetic binder network for stabilizing SiOx/C anodes. ACS Appl. Mater. Interfaces *15*, 49071–49082. https://doi.org/10.1021/acsami.3c08610.
19. Liu, H., Cai, J., Zhou, P., Li, L., Ma, Z., Zhao, X., and Nan, J. (2023). A biomimetic green binder: Forming a biomorphic polymer network in SiOx anode to buffer expansion and enhance performance. Chem. Eng. J. *475*, 146284. https://doi.org/10.1016/j.cej.2023.146284.
20. Qian, G., Chen, X., Lin, H., and Yang, L. (2024). Failure-detecting techniques for commercial anodes of lithium-ion batteries. Cell Reports Physical Science *5*, 102153. https://doi.org/10.1016/j.xcrp.2024.102153.
21. Hoyle, C.E., Lee, T.Y., and Roper, T. (2004). Thiol-enes: Chemistry of the past with promise for the future. J. Polym. Sci. A. Polym. Chem. *42*, 5301–5338. https://doi.org/10.1002/pola.20366.
22. Blasco, E., Wegener, M., and Barner-Kowollik, C. (2017). Photochemically driven polymeric network formation: Synthesis and applications. Adv. Mater. *29*, 1604005. https://doi.org/10.1002/adma.201604005.
23. Davis, A.R., and Carter, K.R. (2015). Controlling optoelectronic behavior in poly(fluorene) networks using thiol-ene photo-click chemistry. Macromolecules *48*, 1711–1722. https://doi.org/10.1021/ma5014226.
24. Gezici, Ö., Durmaz, İ., Bilget Güven, E., Ünal, Ö., Özgün, A., Cetin-Atalay, R., and Tuncel, D. (2014). Dual functionality of conjugated polymer nanoparticles as an anticancer drug carrier and a fluorescent probe for cell imaging. RSC Adv. *4*, 1302–1309. https://doi.org/10.1039/c3ra45120h.
25. Cai, Y., Liu, C., Yu, Z., Ma, W., Jin, Q., Du, R., Qian, B., Jin, X., Wu, H., Zhang, Q., and Jia, X. (2023). Slidable and highly ionic conductive polymer binder for high-performance Si anodes in lithium-ion batteries. Adv. Sci. *10*, 2205590. https://doi.org/10.1002/advs.202205590.
26. Hao, S.-M., Liang, S., Sewell, C.D., Li, Z., Zhu, C., Xu, J., and Lin, Z. (2021). Lithium-conducting branched polymers: New paradigm of solid-state electrolytes for batteries. Nano Lett. *21*, 7435–7447. https://doi.org/10.1021/acs.nanolett.1c02558.
27. Sun, B., Jiao, X., Liu, J., Qiao, R., Mao, C., Zhao, T., Zhou, S., Shi, K., Ravivarma, M., Shi, J., et al. (2024). Neural network inspired binder enables fast Li-ion transport and high stress adaptation for Si anode. Nano Lett. *24*, 7662–7671. https://doi.org/10.1021/acs.nanolett.4c01549.
28. Zhang, J., Yan, L., Zhao, Y., Su, Y., Sun, J., Jiang, H., and Ma, T. (2024). A multifunctional supramolecular polymer binder with hard/soft phase interaction for Si-based lithium-ion batteries. Nano Energy *125*, 109573. https://doi.org/10.1016/j.nanoen.2024.109573.
29. Xu, H., Yang, J., Niu, Y., Hou, X., Sun, Z., Jiang, C., Xiao, Y., He, C., Yang, S., Li, B., and Chen, W. (2024). Deciphering and integrating functionalized side chains for high ion-conductive elastic ternary copolymer solid-state electrolytes for safe lithium metal batteries. Angew. Chem. Int. Ed. Engl. *63*, e202406637. https://doi.org/10.1002/anie.202406637.
30. Yu, X., Liu, J., Wu, J., Ma, S., Luo, Y., and Gao, X. (2024). Three-dimensional dual-layered conductive binder enables stable and high performance of SiOx/C anodes. J. Energy Storage *80*, 110379. https://doi.org/10.1016/j.est.2023.110379.
31. Long, J., He, W., Liao, H., Ye, W., Dou, H., and Zhang, X. (2023). In situ prepared three-dimensional covalent and hydrogen bond synergistic binder to boost the performance of SiOx anodes for lithium-ion batteries. ACS Appl. Mater. Interfaces *15*, 10726–10734. https://doi.org/10.1021/acsami.2c21689.

32. Wu, G., Weng, Z., Li, J., Zheng, Z., Wen, Z., Fang, W., Zhang, Y., Zhang, N., Chen, G., and Liu, X. (2023). Body armor-inspired double-wrapped binder with high energy dispersion for a stable SiOx anode. ACS Appl. Mater. Interfaces *15*, 34852–34861. https://doi.org/10.1021/acsami.3c05228.

33. Li, J., Yang, K., Zheng, Y., Gao, S., Chai, J., Lei, X., Zhan, Z., Xu, Y., Chen, M., Liu, Z., and Guo, Q. (2023). Water-soluble polyamide acid binder with fast Li+ transfer kinetics for silicon suboxide anodes in lithium-ion batteries. ACS Appl. Mater. Interfaces *15*, 30302–30311. https://doi.org/10.1021/acsami.3c05103.

34. Li, Y., Jin, B., Wang, K., Song, L., Ren, L., Hou, Y., Gao, X., Zhan, X., and Zhang, Q. (2022). Coordinatively-intertwined dual anionic polysaccharides as binder with 3D network conducive for stable SEI formation in advanced silicon-based anodes. Chem. Eng. J. *429*, 132235. https://doi.org/10.1016/j.cej.2021.132235.

35. Tang, W., Feng, L., Wei, X., Lai, G., Chen, H., Li, Z., Huang, X., Wu, S., and Lin, Z. (2022). Three-dimensional crosslinked PAA-TA hybrid binders for long-cycle-life SiOx anodes in lithium-ion batteries. ACS Appl. Mater. Interfaces *14*, 56910–56918. https://doi.org/10.1021/acsami.2c19344.

36. Wu, S., Yang, Y., Liu, C., Liu, T., Zhang, Y., Zhang, B., Luo, D., Pan, F., and Lin, Z. (2020). In-situ polymerized binder: A three-in-one design strategy for all-integrated SiOx anode with high mass loading in lithium ion batteries. ACS Energy Lett. *6*, 290–297. https://doi.org/10.1021/acsenergylett.0c02342.

37. He, D., Li, P., Wang, W.A., Wan, Q., Zhang, J., Xi, K., Ma, X., Liu, Z., Zhang, L., and Qu, X. (2020). Collaborative design of hollow nanocubes, in situ cross-linked binder, and amorphous Void@SiOx@C as a three-pronged strategy for ultrastable lithium storage. Small *16*, e1905736. https://doi.org/10.1002/smll.201905736.

38. Liao, H., Liu, N., He, W., Long, J., Dou, H., and Zhang, X. (2022). Three-dimensional cross-linked binder based on ionic bonding for a high-performance SiOx anode in lithium-ion batteries. ACS Appl. Energy Mater. *5*, 4788–4795. https://doi.org/10.1021/acsaem.2c00221.

39. Zhu, C., Chen, S., Li, K., Yin, Z.W., Xiao, Y., Lin, H., Pan, F., and Yang, L. (2023). Quantitative analysis of the structural evolution in Si anode via multi-scale image reconstruction. Sci. Bull. *68*, 408–416. https://doi.org/10.1016/j.scib.2023.01.032.

40. Wang, Z., Li, F., Ding, W., Tang, X., Xu, F., and Ding, Y. (2021). Structural evolution of Si-based anode materials during the lithiation reaction. Nanotechnology *32*, 315707. https://doi.org/10.1088/1361-6528/abfa54.

41. Wu, B., and Lu, W. (2017). Mechanical modeling of particles with active core-shell structures for lithium-ion battery electrodes. J. Phys. Chem. C *121*, 19022–19030. https://doi.org/10.1021/acs.jpcc.7b05096.

42. Tan, J., Matz, J., Dong, P., Shen, J., and Ye, M. (2021). A growing appreciation for the role of LiF in the solid electrolyte interphase. Adv. Energy Mater. *11*, 2100046. https://doi.org/10.1002/aenm.202100046.

43. Chen, J., Fan, X., Li, Q., Yang, H., Khoshi, M.R., Xu, Y., Hwang, S., Chen, L., Ji, X., Yang, C., et al. (2020). Electrolyte design for LiF-rich solid-electrolyte interfaces to enable high-performance microsized alloy anodes for batteries. Nat. Energy *5*, 386–397. https://doi.org/10.1038/s41560-020-0601-1.

44. Wang, Q., Zhu, M., Chen, G., Dudko, N., Li, Y., Liu, H., Shi, L., Wu, G., and Zhang, D. (2022). High-performance microsized Si anodes for lithium-ion batteries: Insights into the polymer configuration conversion mechanism. Adv. Mater. *34*, 2109658. https://doi.org/10.1002/adma.202109658.

45. Wu, F., Dong, Y., Su, Y., Wei, C., Chen, T., Yan, W., Ma, S., Ma, L., Wang, B., Chen, L., et al. (2023). Benchmarking the effect of particle size on silicon anode materials for lithium-ion batteries. Small *19*, e2301301. https://doi.org/10.1002/smll.202301301.

46. Kobayashi, H., Takenaka, Y., Arachi, Y., Nitani, H., Okumura, T., Shikano, M., Kageyama, H., and Tatsumi, K. (2012). Study on Li de-intercalation/intercalation mechanism for a high capacity layered Li1.20Ni0.17Co0.10Mn0.53O2 material. Solid State Ionics *225*, 580–584. https://doi.org/10.1016/j.ssi.2012.02.047.

47. Chen, S., Zheng, G., Yao, X., Xiao, J., Zhao, W., Li, K., Fang, J., Jiang, Z., Huang, Y., Ji, Y., et al. (2024). Constructing matching cathode-anode interphases with improved chemo-mechanical stability for high-energy batteries. ACS Nano *18*, 6600–6611. https://doi.org/10.1021/acsnano.3c12823.